

available at [www.sciencedirect.com](http://www.sciencedirect.com)[www.elsevier.com/locate/brainres](http://www.elsevier.com/locate/brainres)


---



---

**BRAIN  
RESEARCH**


---



---



---

**Research Report**

# Cortical pyramidal cells as non-linear oscillators: Experiment and spike-generation theory

Joshua C. Brumberg<sup>a,\*</sup>, Boris S. Gutkin<sup>b,c</sup>

<sup>a</sup>Department of Psychology, Queens College of the City University of New York, 65-30 Kissena Boulevard, Flushing, NY 11367, USA

<sup>b</sup>Group for Neural Theory, DEC-ENS, Paris and College de France, France

<sup>c</sup>Recepteurs et Cognition, URA CNRS Departement de Neurosciences, Institut Pasteur, Paris, France

---

**ARTICLE INFO**
**Article history:**

Accepted 12 July 2007

Available online 20 July 2007

**Keywords:**

Bifurcation theory

Devil's staircase

Endogenous oscillator

**ABSTRACT**

Cortical neurons are capable of generating trains of action potentials in response to current injections. These discharges can take different forms, e.g., repetitive firing that adapts during the period of current injection or bursting behaviors. We have used a combined experimental and computational approach to characterize the dynamics leading to action potential responses in single neurons. Specifically we investigated the origin of complex firing patterns in response to sinusoidal current injections. Using a reduced model, the theta-neuron, alongside recordings from cortical pyramidal cells we show that both real and simulated neurons show phase-locking to sine wave stimuli up to a critical frequency, above which period skipping and 1-to-x phase-locking occurs. The locking behavior follows a complex "devil's staircase" phenomena, where locked modes are interleaved with irregular firing. We further show that the critical frequency depends on the time scale of spike generation and on the level of spike frequency adaptation. These results suggest that phase-locking of neuronal responses to complex input patterns can be explained by basic properties of the spike-generating machinery.

© 2007 Elsevier B.V. All rights reserved.

---



---

**1. Introduction**

In response to current injections, cortical neurons are capable of generating complex patterns of repetitive discharges. For example, various bursting behaviors (McCormick et al., 1985; Brumberg et al., 2000), sustained constant frequency firing, and adaptive frequency firing (McCormick et al., 1985; Gupta et al., 2000) have all been observed experimentally. Significant experimental and theoretical efforts have been devoted to characterizing the biophysical mechanisms that underlie such repetitive activity (e.g., Llinas et al., 1991; Lampl and Yarom, 1997; Rudy and McBain, 2001; Smith et al., 2000; Izhikevich, 2000).

The presence of such a variety of repetitive discharge patterns suggests that cortical neurons can be considered as non-linear oscillators. Specifically, a class of neurons called regular spiking

cells, and identified as pyramidal neurons (see McCormick et al., 1985), respond to prolonged current injections with sustained trains of action potentials. These neurons are the focus of the present report.

One way to identify the underlying dynamics leading to complex firing patterns is to probe neurons with stimuli that are more complex than constant current injection. This has been done in a variety of neuronal cell classes (Brumberg, 2002; Carandini et al., 1996; Hutcheon et al., 1996; Nowak et al., 1997; Hunter et al., 1998; Volgushev et al., 1998; Fellous et al., 2001). Results suggest that cortical pyramidal neurons can be viewed as non-linear oscillators. Additionally, subthreshold resonances intrinsic to the membrane have significant impact on the response properties of cortical neurons (Llinas et al., 1991; Hutcheon et al., 1996; Hunter et al., 1998). This in turn could

\* Corresponding author. Fax: +1 718 997 3257.

E-mail address: [joshua.brumberg@qc.cuny.edu](mailto:joshua.brumberg@qc.cuny.edu) (J.C. Brumberg).

imply a certain degree of non-linearity in the firing patterns of neurons in response to stimuli of varying frequencies (Richardson et al., 2003). On the other hand, Carandini et al. (1996) reported that near-linear behavior was observed for cortical regular firing cells *in vitro*, with little or no subthreshold resonances evident and only low-pass filtering of sinusoid inputs. Similar data have been reported by Nowak et al. (1997).

We ask the question whether the firing properties of cortical neurons are determined by their spike-generating mechanisms or the resonance properties of their membranes? Using a computational model that does not possess subthreshold resonance properties, we will attempt to characterize a neuron's firing output as a function of its spike-generating machinery.

Our previous results have shown that neocortical pyramidal neurons are capable of following injected sinusoidal inputs up to a critical frequency above which period skipping and 1-to- $x$  phase-locking occurs. We showed that the locking

behavior follows a “devil’s staircase” phenomena, where locked modes are interleaved with irregular firing (Brumberg, 2002). Based on this and similar results in other neuronal (Guttman et al., 1980; Hayashi and Ishizuka, 1992) and excitable systems (Glass et al., 1980), we believe that this behavior can be explained by a specific theory of membrane excitability and spike generation known as type-1 excitability (Hodgkin, 1948; Rinzel and Ermentrout, 1998). To this end, we repeat the experimental protocols on a reduced model, the theta-neuron, which represents a canonical form for type I neural oscillators (for review see Izhikevich, 2000).  $\theta$ -Neurons are characterized by the presence of a saddle-node on an invariant circle bifurcation, a specific point of transition in the dynamics of the membrane voltage that leads to the onset of repetitive firing.

$\theta$ -Neurons have been used to explain the highly irregular interspike interval distributions observed in *in vivo* spike

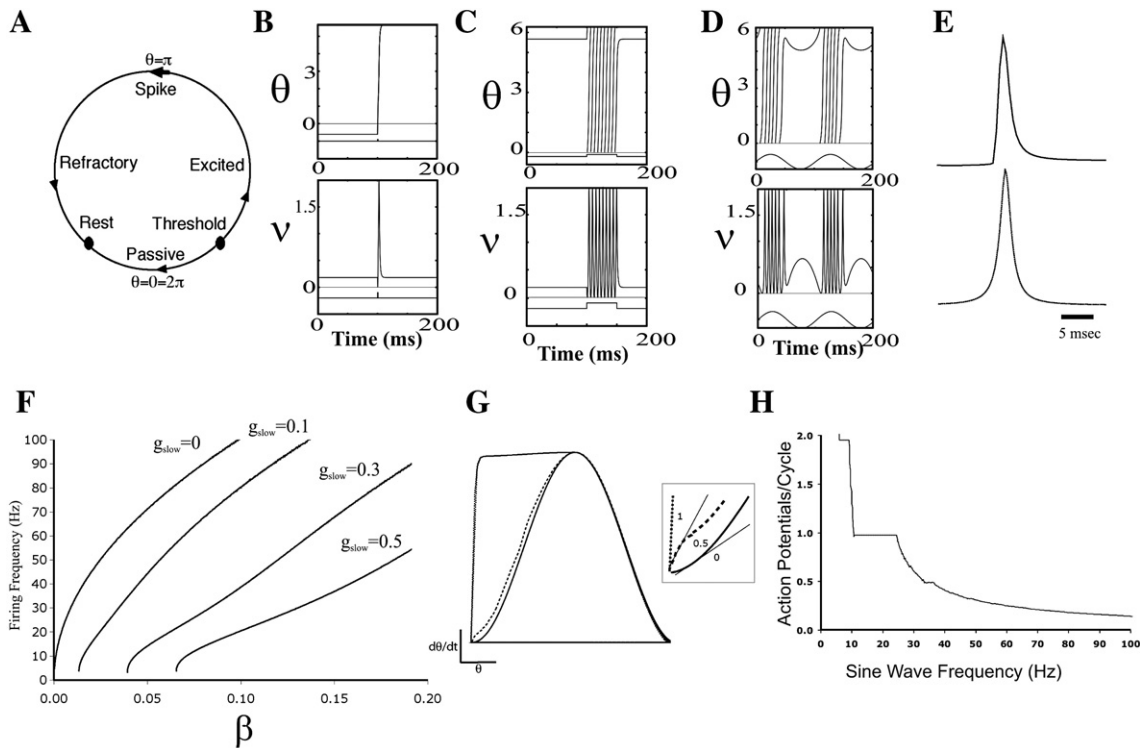


**Fig. 1 – Theta-neuron, a canonical model for type I membrane dynamics.** In the graphs, we show two quantities:  $\theta$ , the phase and  $v = 1 - \cos\theta$  which allows to visualize the spikes. (A) A state diagram for the model showing how the phase dynamics is related to firing stages of a neuron. The rest state is a stable fixed point, once an input pushes the membrane potential past threshold it traverses the entire potential trajectory before returning to rest. (B) Responses of the theta-neuron in the excitable regime to a brief input pulse. (C) Response to a current injection—repetitive firing. (D) Response to injection of sinusoid current (10 Hz), input-dependent bursting. In all panels, the lower traces reflect the input. (E) Influence of the  $I_{Na} = a_{Na}NA$  on the spike onset speed. Example of two spikes one with  $a_{Na} = 0$  and another with  $a_{Na} = 1$ . (F) FI curves for the theta-neuron with various levels of spike frequency adaptation ( $G_m$ ). Note that spike frequency adaptation shifts the plots to the right, decreasing the gain and linearizes the FI curves. (G) Phase-plane for spikes in the augmented  $\theta$ -neuron. Here we plot  $d\theta/dt$  vs.  $\theta$ . Note that the neuron starts at rest  $\theta$  near 0 and rotates through a spike (top of the spike is at  $\theta = \pi$ ). By definition of the phase  $\theta = 0$  is the same as  $\theta = 2\pi$ . The trajectory is equivalent in this parametric space to a spike in the time domain. Trajectories are plotted for  $a_{Na} = 0$  (solid),  $a_{Na} = 0.1$  (dashed) and  $a_{Na} = 1$  (dotted). Note that at the onset of the spike (near  $\theta = 0$ ), higher  $a_{Na}$  leads to a clear increase in the onset sharpness (see inset). This sharpness is quantified by reading off the slope of the trajectory near  $\theta = 0$  (lines in the inset). (H) A detailed phase-locking devil’s staircase for the basic theta-neuron. Here the firing rate is 20 Hz and  $a = 0.01$ . Frequency resolution is 0.1 Hz per data point. Note that this diagram is qualitatively similar to that in Fig. 3, computed with resolution of 1 Hz.

trains (Gutkin and Ermentrout, 1998a,b), precise spike timing to time-varying stimuli *in vitro* (Gutkin, 1999), and an oscillating neuron's response to small pulsatile inputs (Gutkin et al., 2005). Furthermore, the action potential amplitude and width generated by the theta-neuron are largely independent of the injected current amplitude. It is important to note that these intrinsic properties to a large extent have been observed in real cortical neurons *in vitro* and *in vivo* (McCormick et al., 1985; Nowak et al., 2003).

In this report, we show that the frequency locking behavior of the  $\theta$ -neuron in response to sinusoidal input can qualitatively match that of real cortical neurons. Computational studies suggest that this behavior does not depend on the presence of subthreshold oscillatory resonance. We focus on the frequency locking behavior of intrinsically firing cortical neurons and present experimental results from *in vitro* recordings alongside the analogous theoretical analysis. We suggest that identifying the dynamical structure of membrane excitability that leads to

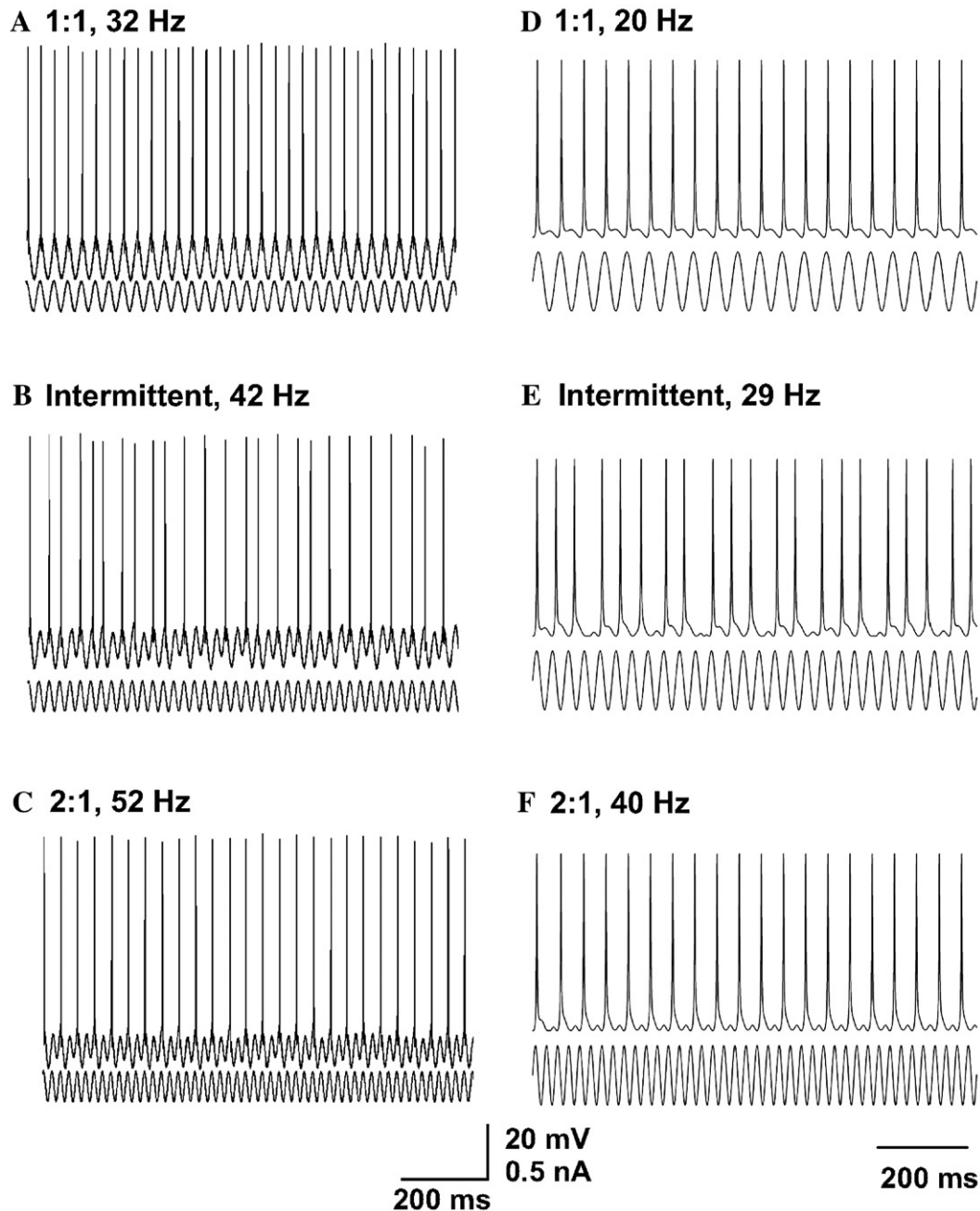


**Fig. 2** – Real and simulated responses to sine wave inputs. Cortical pyramidal neurons show 1:1 phase-locking (A) at low frequencies and then intermittent (B) and 2:1 (C) firing patterns in response to higher-frequency sine waves. Similarly, the theta-neuron shows 1:1 (D), intermittent (E) and 2:1 (F) firing regimes. Parameters for the theta-neuron were:  $\kappa=1$ ,  $\beta$  was set to yield a background firing of approximately 14 Hz:  $\beta=0.0109$ , amplitude of the sinusoid was adjusted to give qualitative match to the experimental data:  $\alpha=0.03$ . The top traces represent membrane voltage and the lower trace is the injected sine wave current.

spike generation in cortical neurons can yield a powerful tool that allows a synthesis of thinking about response properties of neurons.

## 2. Results

Our central finding is that the theta ( $\theta$ )-neuron effectively reproduces the behavior of neocortical neurons in response to sine wave current injections. The theta-neuron is a formal mathematical reduction that derives from a wide class of more complicated neural models that we shall briefly review. A more

detailed treatment is given in [Ermentrout and Kopell \(1984\)](#) or [Hoppensteadt and Izhikevich \(1997\)](#). The theta-neuron came originally from an analysis of the dynamics of cortical pyramidal cells. More generally, the basic requirement for the reduction is that the dynamic behavior of the neural model are of type I excitability (see [Rinzel and Ermentrout 1998](#); [Hansen, 1985](#)). The majority of physiological models for cortical neurons falls into this class and exhibits the following salient characteristics: all-or-none action potentials, repetitive firing that appears with arbitrarily low frequencies, injected current versus firing frequency curves (FI curve) can be readily fitted with a square root (for the instantaneous FI curve) or a linear function (for the

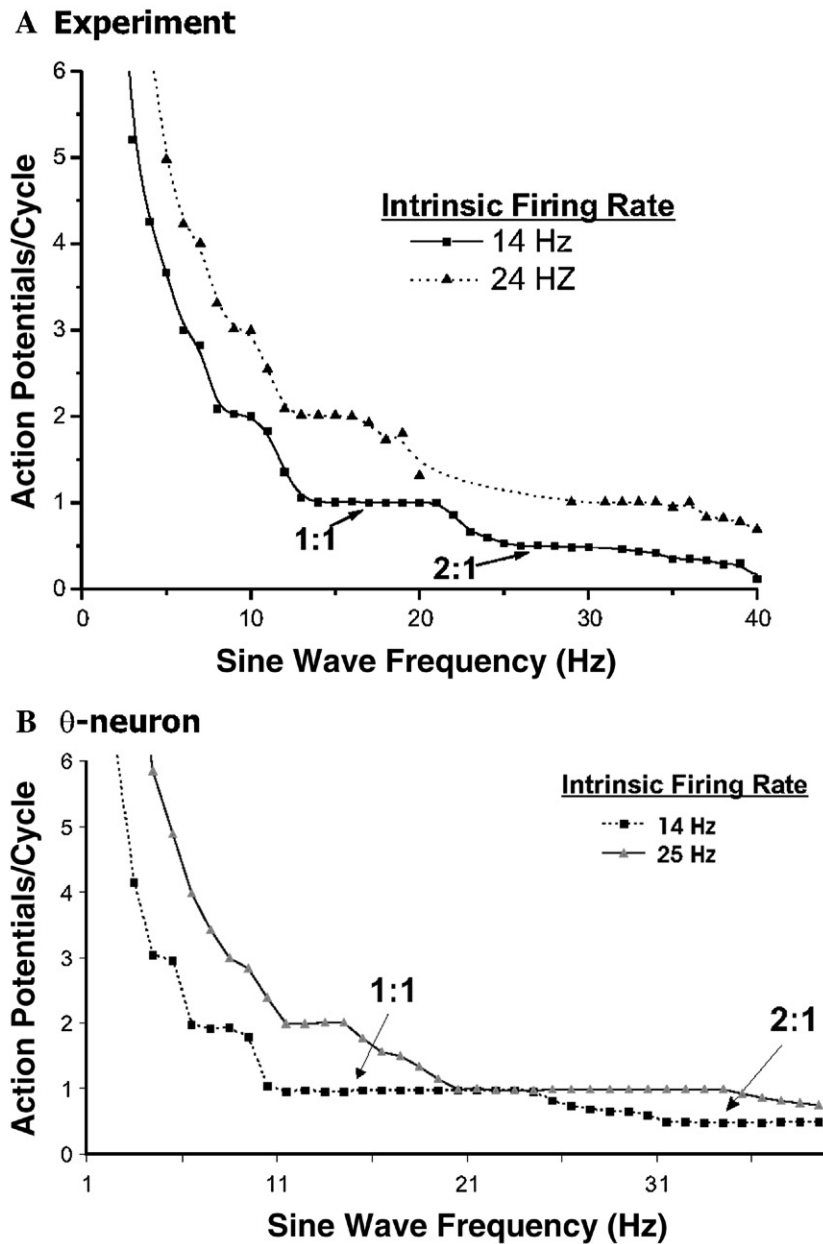


Fig. 3 – Devil’s staircase. Plotting action potentials per sine wave cycle versus the frequency of the injected sine wave reveals multiple whole-number phase-locking regimes (e.g., 1:1, 2:1) in both cortical neurons (A) and the theta-neuron (B). Increasing the basal firing rate in either cortical neurons (A) or the theta-neuron (B) shifts the entire curve to the right leading to an almost twofold increase in frequency range of the 1:1 regime. For the theta-neuron,  $\beta$  was adjusted to give firing rates as marked in figure;  $\kappa = 1$  and amplitude  $\alpha = 0.04$ .

steady-state FI curve). This analysis allows us to reduce a wide class of biophysical models to a simple canonical form that describes the nonlinear characteristics of spike generation and includes the spike itself. Fig. 1 displays the general behavior of the  $\theta$ -neuron model (see Eqs. (11) and (12)). Fig. 1A provides a graphic representation of the model, in Fig. 1B (top) the response of the  $\theta$ -neuron to a suprathreshold transient input is plotted; in response to the input, the phase  $\theta$  makes a procession from 0 to  $2\pi$  (full circle in Fig. 1A). The action potential can be readily visualized by plotting  $v=1-\cos\theta$  (Fig. 1B). Figs. 1C and D show the responses of the  $\theta$ -neuron to prolonged current steps (C) and sinusoid inputs (D) wherein both the  $\theta$  (top panels) and  $v$  (bottom panels) variables are plotted. The speed of the action potential can be varied by adding an additional term  $a_{Na}$  (Eq. (9)); by controlling this parameter (going from 0 to 1), one can speed up or slow down the spike. Fig. 1E gives an example of the two spikes one with  $a_{Na}=0$  and another with  $a_{Na}=1$ . *In vitro* intracellular current clamp recordings were obtained from supragranular pyramidal neurons in response to varying frequencies of sinusoidal input. The pyramidal neurons at low frequencies of sine wave injection, responded with at least one action potential for every cycle of the sine wave (Fig. 2A; i.e. 1:1 phase-locking; see Glass et al., 1980). As the frequency of the injected sine wave is increased, 1:1 phase-locking is lost and the neuron begins to skip cycles, we define this as the intermittent regime and the frequency where 1:1 phase-locking is lost as the critical frequency. The average critical frequency for cortical neurons was  $19.7 \pm 9.7$  Hz ( $n=13$ ) when the steady-state offset was at its minimum (sufficient to just evoke tonic firing). As the frequency is increased further, the neuron enters a 2:1 firing regime (Fig. 2C). Fig. 2 panels A–C (cortical pyramidal neuron) to D–F ( $\theta$ -neuron) show qualitatively how the model captures the biological result. The  $\theta$ -neuron is not intended to accurately capture all the nuances of the biological recordings just the most salient dynam-

ics of the spike-generating machinery of the neuron. As a result, the model does capture the overall firing rate and behavior following sine wave injections. The finding that the  $\theta$ -neuron accurately captures the *in vitro* results argues that the “devil’s staircase” behavior is a consequence of the spike-generating machinery of the neuron and not other cell intrinsic properties which are absent from the theta model. Below we show that the concordance between the experimental data and the model extend over various parameter ranges.

Fig. 1H provides a high-resolution (small-frequency step size) example of the theta-neuron’s response to sinusoidal inputs whereas Fig. 3 compares directly biological data with results from the  $\theta$ -neuron over a range of input frequencies. Note that the results in Fig. 3 are comparable to the results using smaller step sizes (Fig. 1H). In Fig. 3, two different steady-state depolarizing currents were injected *in vitro* to illicit either a 14- or 24-Hz basal firing rate in the same neuron before the sine wave was superimposed. At low firing rates (14 Hz), the neuron displays 1:1 phase-locking up to 22 Hz, then enters the intermittent regime, and finally displays 2:1 phase-locking near 27 Hz. The behavior of the neuron resembles a “devil’s staircase” (e.g., 1:1, 2:1, 3:1, ..., firing regimes interrupted by intermittent firing regimes) which results when an endogenous oscillator is driven by an oscillating input (see Glass et al., 1980; Coombes and Bressloff, 1999). Increasing the basal firing rate (24 Hz) yields similar behavior but shifts the entire curve to the right (dotted line in Fig. 3A). Note that the neuron remains in 1:1 phase lock with the stimulus over an almost twofold greater frequency range for the lower frequency. Similar results were observed in the theta-neuron (Fig. 3B); at a low basal firing rate (6 Hz), the neuron remains 1:1 phase locked between 15 and 25 Hz. Not only was the 1:1 regime dependent on the basal firing rate and the frequency of the sine wave but it was also dependent on the sine wave amplitude. *In vitro* studies revealed that by increasing the

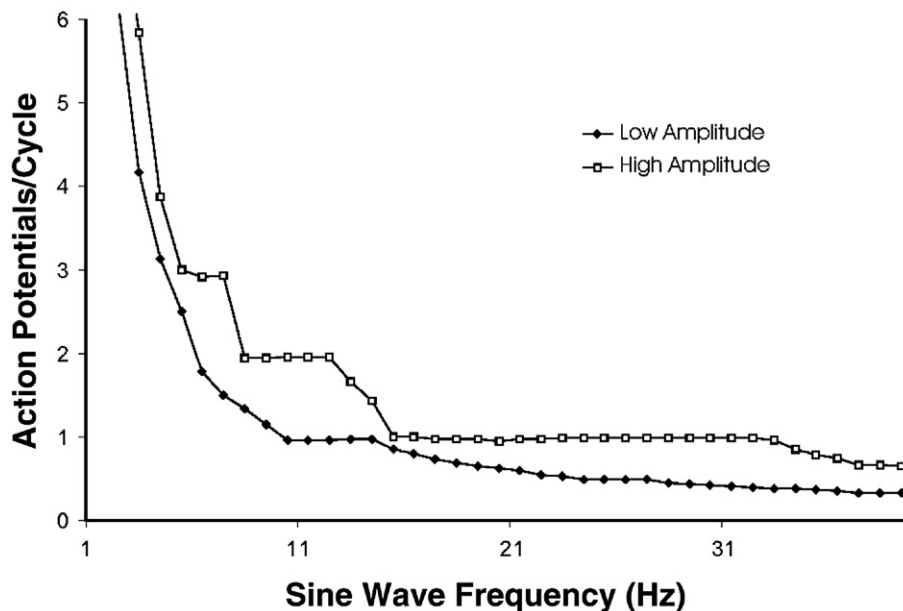
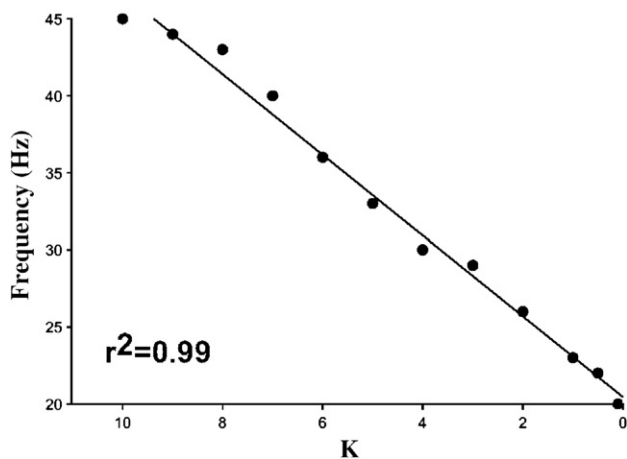


Fig. 4 – Increasing the amplitude of the sine wave expands the 1:1 regime. Plotting action potentials per sine wave cycle versus the frequency of the injected sine wave reveals multiple whole-number phase-locking regimes that are dependent upon the amplitude of the injected sine wave. Here the parameters were:  $\beta$  adjusted to yield a firing rate of 14 Hz, low-amplitude condition:  $\alpha=0.01$ , high-amplitude condition:  $\alpha=0.06$ ;  $\kappa=1$ .

amplitude of the sine wave the neuron's response could be moved from an intermittent regime back to a 1:1 regime ( $n=5$  of 5). The theta model displays similar behavior, increasing the amplitude of the sine wave moved the response curve to the right (Fig. 4) thus increasing 5-fold the range of the 1:1 regime from 3–9 Hz in response to the low-amplitude sine wave to 9–24 Hz in response to the high-amplitude sine wave.

Previously we found that the range and the critical frequency at which 1:1 locking is lost correlated with the half-width of the neurons' action potential but not with its input resistance (Brumberg, 2002). In the  $\theta$ -neuron,  $\kappa$  (Eq. (4)) controls the speed with which the phase variable traverses the firing orbit, and in particular the portion in the spike range (near  $\theta=\pi$ ). The result in varying  $\kappa$  is that the "action potential" width effectively varies; a large  $\kappa$  is akin to a narrow action potential. Fig. 5 demonstrates the relationship between  $\kappa$  and the critical frequency. The critical frequency wherein the theta-neuron could no longer respond 1:1 was tightly correlated to  $\kappa$ , simulations with larger  $\kappa$  values had higher critical frequencies than simulations with lower  $\kappa$  values, this relationship was highly significant ( $r^2=0.99$ ). Taken with the biological data described above, these results strongly suggest that the spike-generating mechanism and not the passive cell properties are crucial to the phase-locking behavior of cortical pyramidal cells.

The  $\theta$ -neuron is a canonical model for type I spike-generators. Results from the  $\theta$ -neuron, therefore, should match those generated by conductance-based models that are also type I. To illustrate this, we compared the responses of our  $\theta$ -neuron to a single-compartment conductance-based model of a pyramidal neuron used previously by others (Traub et al., 1999; also see Appendix A). Indeed a more "biologically realistic" model displays devil's staircase type behavior (Fig. 6A) as expected. Looking at a wide range of input frequencies both the conductance-based



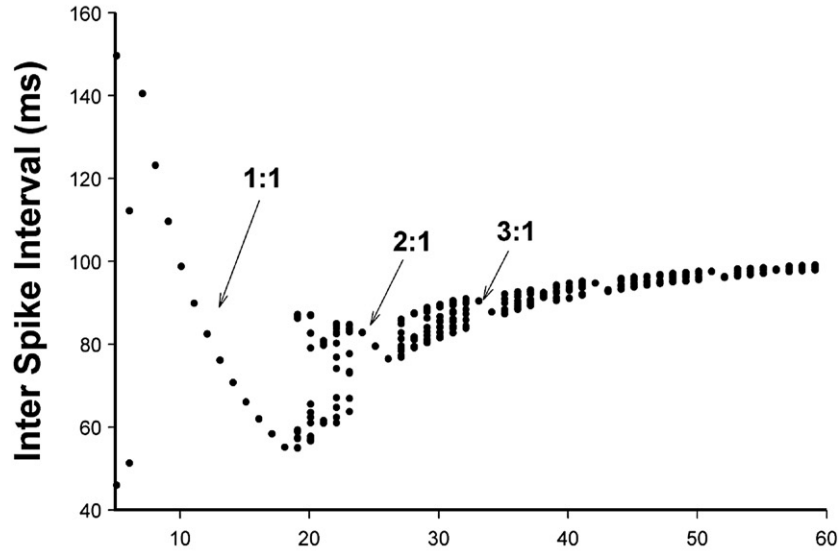
**Fig. 5 – Spike width is correlated with the loss of 1:1 phase-locking. Increasing the velocity in which the theta-neuron traverses its orbit decreases the width of the spike and this enables the theta-neuron to respond in a 1:1 fashion to a greater range of frequencies. Plotted is the critical frequency, the frequency where 1:1 firing is lost versus  $\kappa$  as  $\kappa$  increases the critical frequency increases, Note that the x-axis is inverted. Here  $\beta$  was set to give a background firing rate of approx. 10 Hz, amplitude of the sinusoid;  $\alpha=0.05$ .**

model (Fig. 6A) and the  $\theta$ -neuron (Fig. 6B) show whole-number phase-locking (1:1, 2:2, 3:1) that is interrupted by intermittent regimes. The  $\theta$ -neuron show a much narrower locking regimes and also the action potential duration is a bit more variable for the  $\theta$ -neuron leading to apparent multiple points in the plot in the 1:1 regime. However it is clear that the canonical model predicts the qualitative behavior of the real neuron as well as of the more complex conductance-based model.

In order to further corroborate our proposal that it is the active spike-generating machinery that has the predominant effect on the critical frequency of the neuron, we examined how the onset spike-speed changes the locking. For this, we used a further extended  $\theta$ -neuron (see Eqs. (13), (14), and (15)). This model includes a Na-like current that allows us to control the speed with which the spikes rise off the floor by controlling the strength of this "current" (see Fig. 1F). We further define a spike-onset-speed parameter by using a phase-plane method (see Experimental procedures). Fig. 7A shows an example of ISI/freq plot for two speeds of the spike; slow:  $\alpha_{Na}=0$  – the classical  $\theta$ -neuron and fast:  $\alpha_{Na}=1$ . Clearly the faster spike generation leads to a right-ward shift in the locking graph with the faster action potential locking at higher frequencies than the slower one. The neuron with the slower initiation of its action potential ends its 1:1 locking regime at approximately 13 Hz, whereas the neuron, which initiates its action potential faster, can maintain the 1:1 regime up to 35 Hz. As the action potential is initiated quicker the critical frequency wherein the 1:1 regime is lost increases (Figs. 7B, C).

A further prominent process that controls the excitability of the neuronal membrane is spike frequency adaptation most often produced by slow voltage-dependent potassium currents. As is the case for pyramidal cells, the level of spike frequency adaptation has a significant effect on  $\theta$ -neuron's phase-locking behavior. In cortical pyramidal neurons, the spike frequency adaptation (SPA) is due to slow voltage-dependent potassium currents, such as I-AHP and I-M. Here we used the adapting  $\theta$ -neuron to study the effects of spike frequency adaptation on the locking patterns of tonically firing neurons driven by a sinusoidal inputs. As described above, the basal firing rate of the neuron was determined by a DC current injection then a pre-set amplitude sinusoid was injected and locking patterns examined. In Fig. 8A, we see the devil's staircase behavior for the  $\theta$ -neuron biased to fire at a 20-Hz steady-state firing rate. Note that the most obvious effect of the spike-frequency adaptation is to shift the curves to the left – decreasing the maximal input frequency at which the neuron is 1:1 locked. However SPA shows another and unexpected effect – the neuron is more likely to lock at higher modes: 2:1 and 3:1 for example when the adaptation variable is set to a low level ( $g_{slow}=0.5$ ). Analogous results are seen for the conductance-based model (Fig. 6B). In fact if we to compare the firing of the  $\theta$ -neuron without adaptation ( $g_{slow}=0.00001$ ) and with adaptation ( $g_{slow}=0.5$ ) to a sinusoid input of 55 Hz, we see that the non-adapting cell is not locked to the stimulus (Fig. 9A, top) and the firing phase varies, meaning that the overall timing of action potentials are still modulated by the sinusoidal current pulse but they are not phase locked and occur at pseudo-random phases (Fig. 9A, bottom). On the other hand, the adapting neuron locks to the 55 Hz input at 2:1 mode, and the input-firing phase plot shows that the spikes are phase-locked to the stimulus (Fig. 9B), at higher frequencies the neurons skips input cycles, but

**A Conductance Based Model**



**B  $\theta$ -neuron**

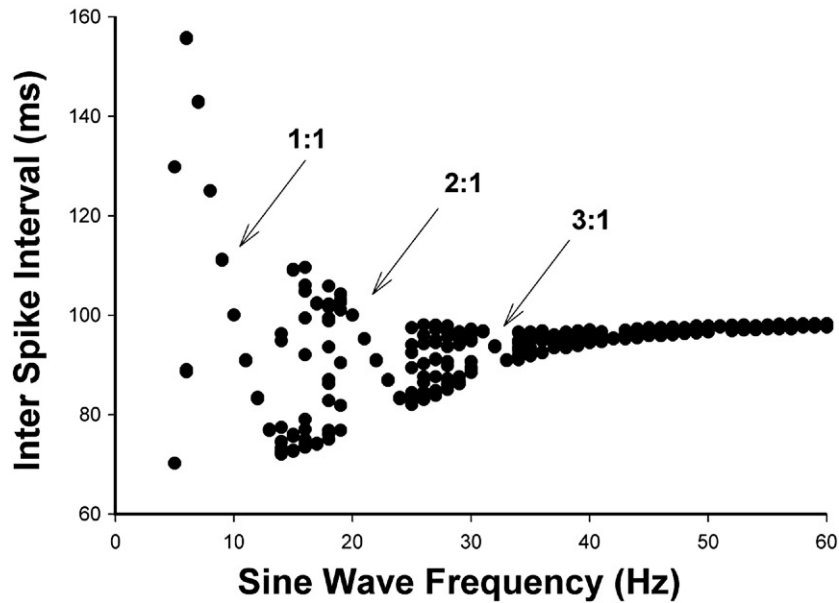
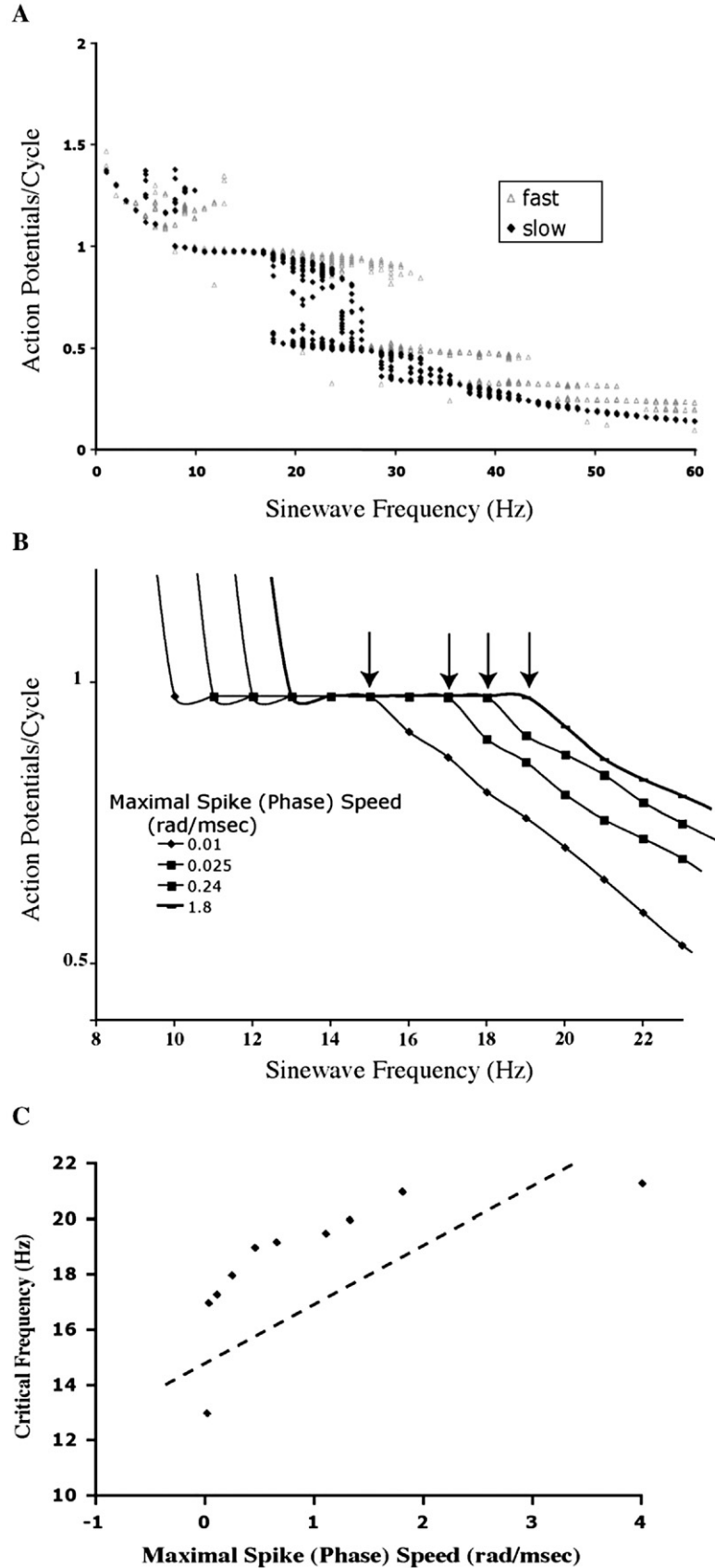


Fig. 6 – Type I neuronal oscillators show devil’s staircase phenomena. Both a “realistic” type I neuronal oscillator (A) and the theta-neuron (B) respond similarly to sine wave inputs. Here we plot a periodogram for both models: the inter-spike intervals collected for a simulation of 1000 ms are plotted for each value of the sinusoid input frequency. Parameters for the conductance based model are as in Appendix A, except that the amplitude of the DC current was adjusted to yield a 10 Hz firing rate. For the theta-neuron:  $\kappa = 1$ ;  $\beta$  adjusted to give a firing rate of 10 Hz;  $\alpha = 0.01$ . The choice of  $\alpha$  was motivated purely to give a qualitative match to the conductance-based model graph, other values of  $\alpha$  yield similar devil’s staircase results with shifted critical frequency (simulations not shown).

Fig. 7 – Spike onset speed influences the phase locking. We use the augmented theta-neuron to examine how the speed of the spike onset influences the locking to sinusoidal inputs. (A) Shows the raw locking diagrams for two spike speeds. Fast is when  $a_{Na} = 1$  and slow is when  $a_{Na} = 0$ . Note a clear shift to higher frequencies for the faster spike onset speed. (B) Devil’s staircases (see Experimental procedures) for several spike speeds (marked on the graph). Arrows indicate the critical frequency at which the 1:1 locking is lost. (C) The critical frequency is correlated with the spike onset speed (dashed line showing the trend). Here the neuronal firing rate with no sinusoidal input is at 15 Hz.

when it fires, it does so at a fixed input phase. In fact, spike-frequency adaptation appears to expand the range of frequencies at which the neuron is able to lock to the stimulus.

We can further understand why the spike frequency adaptation expands the locking regime by considering theoretical models of neural oscillators and appealing to phase



model arguments. While the formal mathematical treatment is beyond the scope of this report, we shall outline a heuristic argument. Given that the neuron in question is firing periodically, as is the case here, it can be described by a phase of its firing. This phase rotates uniformly in time, hence for the neuron a phase model can be written down.

$$D\phi/dt = \omega + \text{PRC}(\phi)I \quad (1)$$

Here  $\theta$  is the “phase” of the neural membrane potential along its firing cycle (with the spike occurring when  $\theta = \pi$ ),  $\omega$  is the frequency of the oscillator (and it can be shown that  $\phi = \omega t$ ),  $I$  is the periodic input and PRC is the infinitesimal phase response function (PRC) of the oscillator (see [Ermentrout, 1996](#) for further definition). The phase–response curve reflects how the phase of the oscillation is perturbed, or affected by an arbitrarily weak and brief stimulus. The PRC tracks the relationship between the relative timing (phase) of the input and the phase shift produced (the response). This is analogous to the standard impulse–response function. Given the inputs are sufficiently weak (meaning they do not produce extra spikes but only shift spike times), inputs that are more complex than the impulse yield phase responses that are a linear superposition of the PRC. The internal biophysics of the spike-generating machinery of the neuron is reflected in the phase model above through the phase–response curve –  $\text{PRC}(\phi)$ . Note that the challenge is to find a mathematical transformation that takes the state variable of the neuron (e.g., the voltage) and the phase  $\phi$  into account. In general, this is not easy, but for neural oscillators, it can be shown that such a transformation exists (see [Hoppensteadt and Izhikevich, 1997](#) for proof). [Fig. 10](#) gives two examples of PRCs for a non-adapting theta-neuron ([Fig. 10A](#)) and another PRC for an adapting theta-neuron ([Fig. 10B](#)). Note that the PRC for the non-adapting neuron is purely positive and symmetric which demonstrates that the cell’s spike-times are advanced by inputs throughout its firing cycle. For an adapting case, the PRC has strong skew to the right and a negative region as has been shown before ([Gutkin et al., 2005](#)). This behavior is linked to changes in the underlying spike generation mechanism(s) ([Ermentrout et al., 2001](#)). Hence, for these types of neural oscillators, excitatory inputs at the beginning of the firing cycle actually delay the subsequent spike (see [Gutkin et al., 2005](#) for further discussion). The negative region and skew in the PRC means that excitatory inputs delay the spike time (lengthen the interspike interval) at the beginning of the firing cycle and advance the spike times (lengthen the interspike interval) at the end of the firing cycle. If the input is periodic, we can define a phase for it ( $\phi_1$ ) and rewrite the phase model as a phase difference model between the firing phase and the input phase.

$$\begin{aligned} d\psi/dt &= d(\phi - \phi_1)/dt \\ &= -d\phi_1/dt + \omega + \text{PRC}(\phi)I \end{aligned} \quad (2)$$

Now the phase  $\phi_1 = \omega_1 t$ , so the equation becomes

$$D\psi/dt = \omega - \omega_1 + \text{PRC}(\phi)I \quad (3)$$

The phase-locking will occur when the derivative on the right-hand side is 0. Hence the condition is:

$$\omega_1 - \omega = \text{PRC}(\phi)I$$

Note that the left-hand side is a difference in the frequencies of the input and the output. Previously, it has been shown that the neuronal oscillators with purely positive PRCs are likely to lock only to stimuli with frequencies above the natural frequency of the oscillator (e.g., see [Glass and Mackey, 1988](#); [Izhikevich, 2007](#)). Therefore, with a purely positive PRC, the input can only accelerate the firing, hence only increase  $\omega$ . With a purely positive PRC (e.g., [Fig. 10A](#)), the right-hand side of Eq. (3) is positive; hence the equality can hold only when the input frequency is larger than the intrinsic frequency of the oscillator. Lower-frequency inputs cannot slow down the firing frequency making 1:1 locking unlikely. On the other hand, oscillators with biphasic PRCs can lock to both higher and lower input frequencies (e.g., [Fig. 10B](#)). The lower-frequency stimuli will have a chance to appear at phases when the PRC is negative for (some frequencies). The net result of this is to slow down the firing to fire only a single spike per input cycle and hence drive the difference towards zero inducing 1:1 phase-locking to the stimulus. More precisely the right-hand side of Eq. (3) can be negative, hence equality can happen when the input frequency is below the intrinsic one. Note that here we give a heuristic argument only for 1:1 locking, however similar arguments can work for higher locking modes (see [Glass and Mackey, 1988](#)). Also note that an important caveat of this argument is that the intrinsic firing frequency of the neural oscillator must be sufficiently close to the input frequency.

More formal proofs have been described using Poincaré map methods and computing or estimating the borders of the Arnold tongues associated with the various locking modes. While such more formal proofs (e.g., [Coombes and Bressloff, 1999](#)) are beyond the scope of this report, we can use a heuristic approach to link the PRC shape to the relative size of the locking regions. Here we followed the method suggested by [Schaus and Moehlis \(2006\)](#) based on averaging arguments and Fourier expansion of the PRC. Omitting full formal details of the methods (but see [Schaus and Moehlis, 2006](#)), we use the fact that for type I neurons near the bifurcation leading to the onset of repetitive spiking, the PRC is  $(K/\omega)(1 - \cos\theta)$  ([Ermentrout, 1996](#); [Brown et al., 2004](#)). Here  $K$  is a constant that depends on the model particulars and  $\omega$  is the intrinsic frequency of the oscillation. Following [Schaus and Moehlis \(2006\)](#), we can show that the 1:1 Arnold tongue boundary is given by:

$$\frac{\omega}{\nu} - 1 = \pm \frac{a_{AC}K}{2\omega\nu} \quad (4)$$

If we want to plot this boundary in the firing rate/amplitude plane, we only need to solve it for  $\omega$ :

$$\omega = \pm \frac{a_{AC}K}{2\nu} + \nu \quad (5)$$

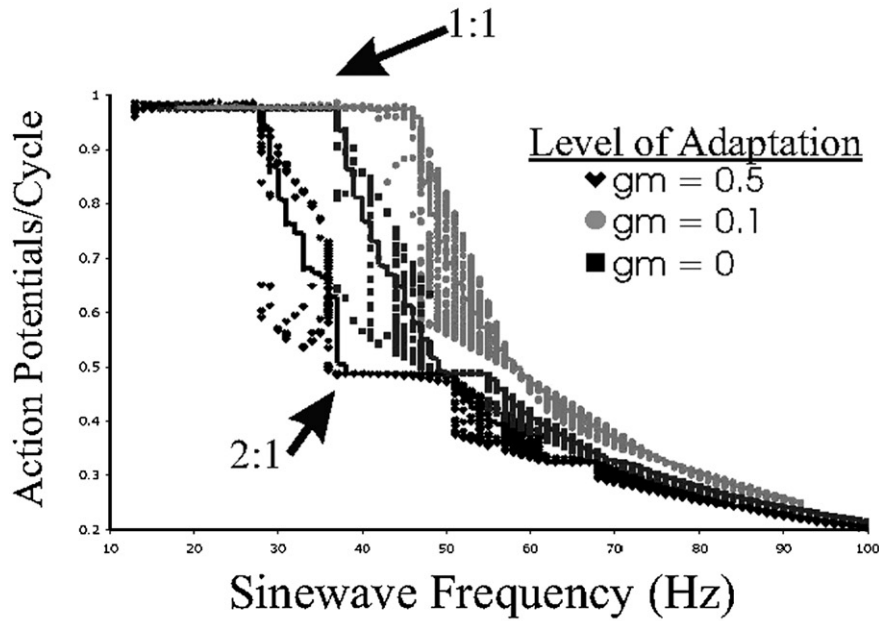
For higher locking  $n$ :1 modes, this equation becomes:

$$\omega = \pm \frac{a_{AC}K}{2\nu} + \frac{1}{n}\nu \quad (6)$$

For type II neurons, hence strongly adapting neurons (see above and [Gutkin et al., 2005](#)), the PRC can be approximated by:

$$\text{PRC}(\theta) = \frac{C_b}{\omega - \omega_{SN}} \sin(\theta - \phi_B) \quad (7)$$

**A  $\theta$ -neuron**



**B Conductance Based Model**

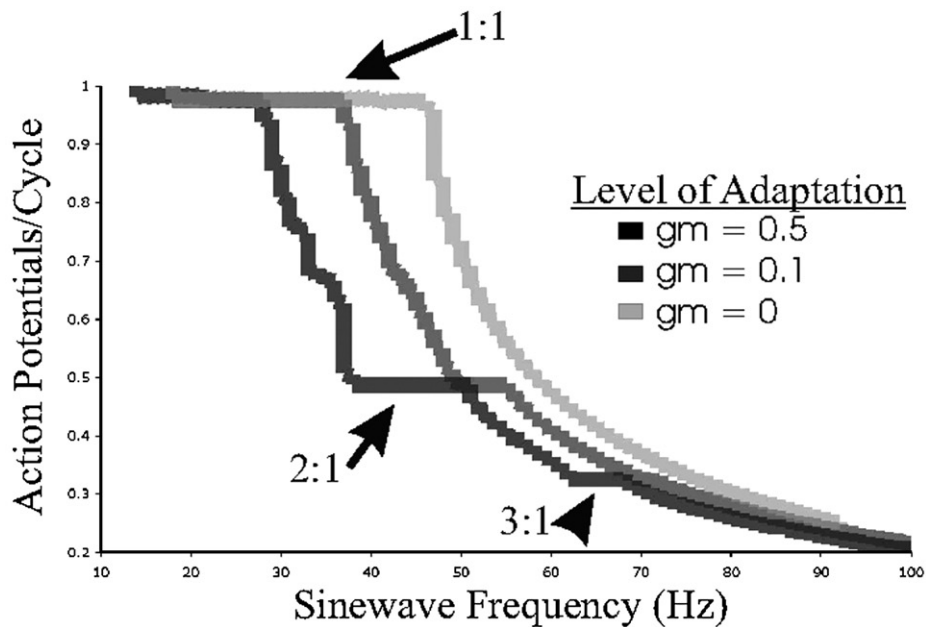


**Fig. 8 – Spike frequency adaptation sculpts the devil’s staircase, carving higher mode-locking regimes. (A) Devil’s staircase for three levels of adaptation in the  $\theta$ -neuron biased to fire at 20 Hz. Note that with adaptation, the frequency range of 1:1 locking moves to lower input frequencies. However, higher locking regimes (2:1, 3:1) tend to expand in the stronger adapting cases. (B) Results for a conductance-based model. Here we use the type I neural oscillator model as in Fig. 6. We change  $g_{slow}$  to control the level of spike frequency adaptation and re-adjust the DC current to re-equilibrate the firing rate to 20 Hz. We show two examples of devil’s staircase behavior, one with  $g_{slow}=0$  and second with  $g_{slow}=1$ . Note that the results of the conductance-based model follow qualitatively the theta-neuron.**

Here  $C_b$ ,  $\omega_{SN}$  and  $\phi_B$  are constants determined from the models (see Brown et al., 2004):  $\omega_{SN}$  is the minimal firing rate (frequency of the oscillations at the bifurcation), the other two constants are determined directly from the specific Hodgkin-Huxley type model. Hence for such type

of dynamics, the 1:1 Arnold tongue boundaries are given by:

$$\frac{\omega}{v} - 1 = \pm \frac{a_{AC}|C_B|}{2v|w - w_{SN}|} \tag{8}$$

or in the  $\omega$ - $a_{AC}$  plane:

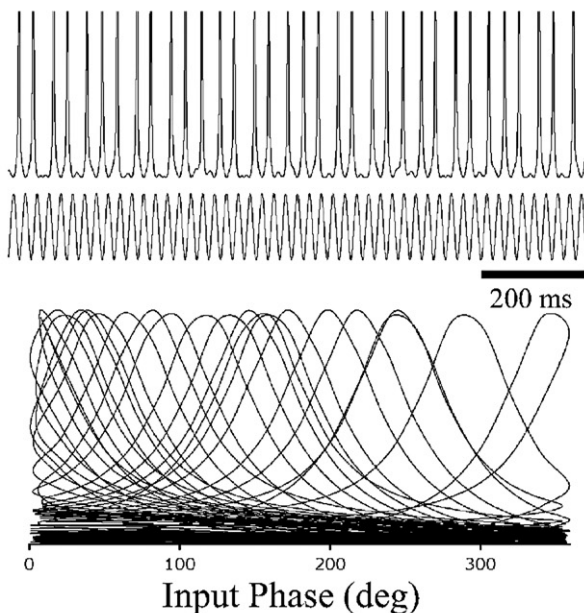
$$\omega = \pm \frac{a_{AC}|C_B|}{2|w - w_{SN}|} + \nu \quad (9)$$

and higher-order  $n:1$  locking borders are given by:

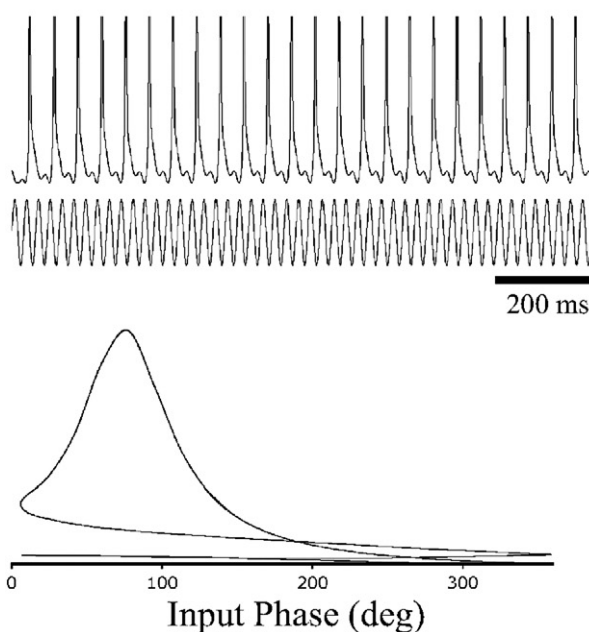
$$\omega = \pm \frac{a_{AC}|C_B|}{2|w - w_{SN}|} + \frac{1}{n}\nu. \quad (10)$$

Now we can briefly comment on the different bifurcation types and the width of locking regions. Assuming that the constants  $C_B$  and  $K$  are on the same order of magnitude (or perhaps even approximately equal), we observe that for a subcritical bifurcation, the minimal firing frequency is non-

### A $\theta$ -neuron without adaptation



### B $\Theta$ -neuron with adaptation



zero, hence the denominator of Eq. (10) is less than the denominator of Eq. (6); this implies clearly that the area bounded by the 1:1 tongue borders for the type II case is larger than for type I. This gives further support for the arguments above and the numerical simulations.

## 3. Discussion

In this report, we considered spiking patterns in the responses of cortical neurons *in vitro* to an injected periodic stimulus. Such response patterns form a devil's staircase structure, with regular phase locked and irregular intermittent frequency ranges. We further investigated if such patterns can be reproduced by a canonical model of spike generation in type I neural membranes; the  $\theta$ -neuron. In general, our results show that the  $\theta$ -neuron can reproduce the devil's staircase behavior of the cortical neurons both qualitatively and, quantitatively, dependent on parameter choices. The behavior of the  $\theta$ -neuron is general for a class of models that exhibit type I membrane dynamics (see Rinzel and Ermentrout, 1998), and indeed, a detailed conductance-based model of cortical neurons showed behavior nearly identical to that of the  $\theta$ -neuron. Crucially, the fact that  $\theta$ -neuron can replicate the biological results, including the dependence of the critical frequency on the spike-width, argues strongly that it is the spike-generating machinery that determines the frequency-response properties of the neurons.

Furthermore by identifying the parameter in the  $\theta$ -neuron that determines the "half-width" of the spike, we were able to account for experimental observation that the critical frequencies for onset of the phase-locked and intermittent regimes depend of the spike half width and not on input resistance. Similarly we were able to augment the theta-neuron to include a process that controls the sharpness of the spike onset. This parameter was also positively correlated with the critical frequency: the sharper the spike (faster spike onset) the higher is the critical frequency of 1-1 locking. These two last points imply that the locking properties of neurons depend mostly on the behavior of the active channels that underlies spike generations and not on the passive properties. Note that such dependence cannot be predicted from simple integrate-and-fire neuron models, and is also in agreement with recent theoretical results of Fourcaud-Trocme et al. (2003), that linked the critical cut-off response frequency to noisy stimuli to the dynamics of spike onset.

**Fig. 9 – Spikes and phases with various levels of adaptation in the theta-neuron biased to fire at 20 Hz basal rate. The input frequency (55 Hz) was chosen to exhibit the locked (with adaptation) and unlocked (without adaptation) firing regimes. Amplitude of the sinusoid was 0.03. In each panel, the upper graph shows the spikes with the sinusoid inputs (lower trace). The lower panel shows the  $\nu$  (pseudo-voltage) sinusoid-phase phase-plane. Note that a single limit cycle in this space means a phase-locked solution. (A)  $g_{slow}=0$ . Note that at this input frequency for this sinusoid amplitude, the firing is not phase-locked and is irregular. The phase-plot show that the spikes come at a wide range of input phases. (B)  $g_{slow}=0.5$ . Here the spikes are 2:1 locked to the stimulus and the phases are the same for all the spikes. The adapting theta-neuron is phase-locked to this stimulus.**

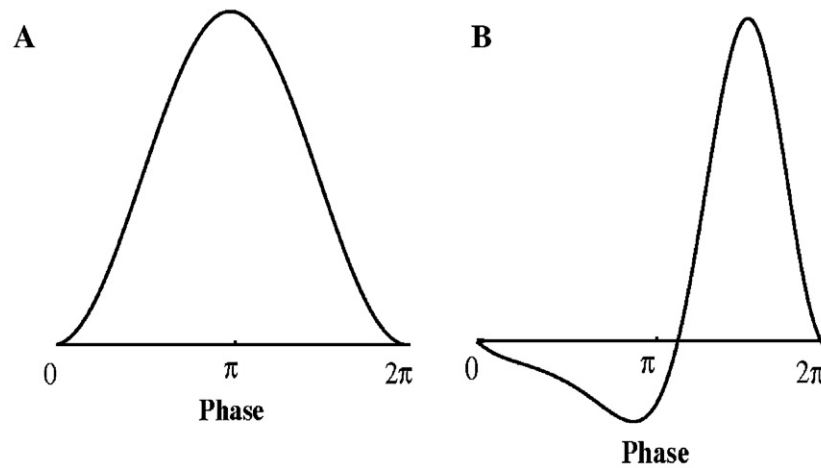


**Fig. 10 – Phase–response curves for non-adapting and adapting theta-neuron models. Neuron is firing at 20 Hz. Here we plot a normalized infinitesimal PRC (see Ermentrout et al., 2001 for precise methods). The y-axis gives the change in the firing phase, positive is phase advance and negative is phase delay. (A) PRC with no adaptation ( $g_{\text{slow}}=0$ ): it is symmetric and purely positive. (B) PRC with adaptation. Note the skew and the negative region ( $g_{\text{slow}}=4$ ).**

We also note that type I dynamics imply that there is no subthreshold resonances and indeed the  $\theta$ -neuron does not have any subthreshold oscillations. Previously, complex spiking responses have been tied to the presence of subthreshold oscillations (e.g., Fellous et al., 2001; Desmaisons et al., 1999; Amitai, 1994; Llinas et al., 1991). Indeed the Hodgkin–Huxley model can also display devil’s staircase behavior; however, it has been argued that it arises due to resonances inherent in the membrane excitability dynamics (e.g., Holden, 1976; Parmananda et al., 2002). Since the  $\theta$ -neuron yields regular (locked) and irregular responses dependent on input frequency, the link between subthreshold oscillations and complex firing patterns is not quite as straightforward as previously suggested. Perhaps the subthreshold resonances become important under specific input regimes, when the inputs drive the cell membrane into the voltage ranges spanned by the oscillation as suggested in Richardson et al. (2003). In any case, our results clearly demonstrate that complex spike locking patterns and intermittency is not equal to impedance resonances, band-pass filtering or strong subthreshold oscillations.

Richardson et al. (2003) showed that the effects of subthreshold resonance is apparent in spiking responses when the sinusoid falls into the subthreshold region. The cell fires due to random variations in the noisy synaptic inputs. The sinusoid then modulates the overall probability distribution of spike times and this is combined with the intrinsic membrane resonance. In the present study, we examined a different regime, where the cell is biased to be above its firing threshold and then the sinusoid modulates its firing. In this regime, the  $\theta$ -neuron is valid (since the reduction presupposes that the neuron is near its bifurcation) and the neural membrane is sufficiently depolarized from rest where subthreshold resonance and/or oscillations are present. Arguably, this regime is more like the situation *in vivo* where the neurons are strongly depolarized by background synaptic inputs and tend not to show resonant behavior (see Carandini et al., 1996).

Alexander et al. (1990) developed a coherent theoretical approach to study the phase-locking behavior in excitable systems with type II excitability. They showed by formal analysis that both locking and intermittency can occur in such neurons when

they are in the excitable regime (at rest without the sinusoidal forcing) and, furthermore, that the qualitative picture persists into the oscillatory regime. In the intermittent regions, simulations of the Fitzhugh–Nagumo model suggest chaotic behavior with typical period doubling bifurcations. While a full comment on the detailed analysis carried out in that work is beyond the scope of this report, we can point out that one clear difference with the case considered here and the previous report is that in type II systems considered by Alexander et al. (1990), the voltage trajectories during spiking may have different amplitudes. Hence the periodic forcing in that system can modify not only the frequency of the firing but also the shape of the spikes. This is clearly absent in type I excitable neural models, and by definition in the theta-neuron considered here. However, the qualitative picture of phase-locking and intermittency, hence the devil’s staircase is similar in the two cases. We thus would speculate that the structure of bifurcations separating the various regions on the staircase is also similar between the case considered in Alexander et al. (1990) and for type I systems. In principle, methods developed by Alexander and colleagues may be applied to the theta-model to identify the saddle-node on an invariant circle bifurcations separating phase-locked solutions from intermittent firing and the period-doubling in the intermittent regions; however, such detailed mathematical analysis is beyond the scope of this report.

We believe that this report can be combined with the results in Richardson et al. (2003) to begin to synthesize a coherent picture of when and how neurons respond to their inputs in a network setting. Therefore, when the average membrane potential of the neuron falls within the operating range of the currents that underlie subthreshold oscillations (e.g., slow potassium currents, see Hutcheon and Yarom, 2000 for review), and the neuron fires due to the synaptic input, resonances can be observed in the spiking pattern. On the other hand, when the neuron is depolarized by background synaptic events to fire repetitively, the frequency locking behavior of the neuron is determined by the spike-generating properties (for example, the spike half-width and the speed of spike onset).

### 3.1. Why is it important to determine which class of bifurcation underlies spike generation in cortical neurons?

Recent developments in *in vitro* and *in vivo* electrophysiological techniques have led to an increase in the detailed data available on the properties of neural membranes. Modeling literature has followed in the footsteps of these data explosion with biophysically explicit models that focus on the details (currents, morphology, etc.) of individual neurons identified in experimental settings (e.g., Borg-Graham, 1998; Destexhe et al., 1996; Mainen et al., 1995). Such models are then used to make specific predictions for response properties of neurons. Another modeling approach is to use extremely simple models of either single neurons or populations of neurons in order to study possible dynamics and behaviors of circuits or networks of neurons. Building on a rich history of reduced conductance-based models (e.g., Fitzhugh–Nagumo, Morris–Lecar) general mathematical principles relating biophysical models of cortical neurons to reduced and canonical models of spike generation in cortical neurons are beginning to be elaborated and tested on neuronal data e.g., spike response models (Gerstner and Kistler, 2002); the various versions of non-linear integrate and fire models (Richardson et al., 2003; Fourcaud-Trocme et al., 2003), and more general dynamical systems approaches (Izhikevich, 2000). We suggest that identifying the dynamical structure of membrane excitability that leads to spike generation in cortical neurons can yield a powerful tool that allows a synthesis of thinking about response properties of neurons.

## 4. Experimental procedure

### 4.1. Preparation of acute brain slices

The methods used to prepare brain-slices have been presented in detail elsewhere (Brumberg et al., 2000; Brumberg, 2002). Briefly, coronal slices (400  $\mu\text{m}$  thick) of primary visual cortex were obtained from male or female ferrets 4–7 months old (Marshall Farms) using a DSK microslicer (Ted Pella, Inc.). The ferrets were deeply anesthetized with sodium pentobarbital (30 mg/kg) and decapitated. The brain was quickly removed and the hemispheres separated with a midline incision. During the preparation of the cortical slices, the tissue was kept in a solution where NaCl had been replaced with sucrose while the osmolarity was maintained at 307 mosM. After preparation, the slices were maintained in an interface style chamber (Fine Scientific Tools) and allowed to recover for at least 2 h at 34–36 °C. The bathing medium contained (in mM): 124 NaCl, 2.5 KCl, 2  $\text{MgSO}_4$ , 1.25  $\text{NaH}_2\text{PO}_4$ , 1.2  $\text{CaCl}_2$ , 26  $\text{NaHCO}_3$ , 10 dextrose and was aerated with 95%  $\text{O}_2$ , 5%  $\text{CO}_2$  to a final pH of 7.4. For the first 10 min that the slices were in the recording chamber, the bathing medium contained an equal mixture of the bathing and slicing solutions with 2.0 mM  $\text{CaCl}_2$  which was subsequently reduced to 1.2 mM in the bathing solution, an extracellular  $\text{Ca}^{2+}$  concentration similar to what has been observed in cats *in vivo* (Hansen, 1985).

### 4.2. Electrophysiology, data collection and analysis

All recordings were obtained from the supragranular layers of ferret visual cortex. Once a stable intracellular recording

had been obtained (resting  $V_m$  of  $-60$  mV or more negative, overshooting action potentials, ability to generate repetitive spikes to a depolarizing current pulse), the cell was classified according to its discharge pattern in response to an injected current pulse (120 ms, +0.5 nA) as intrinsically bursting, regular-spiking, fast-spiking or chattering (McCormick et al., 1985; Brumberg et al., 2000); all neurons in the present analysis were characterized as regular spiking ( $n=13$ ). To approximate the more depolarized membrane potentials observed *in vivo* a small depolarizing current was injected (0.2–0.7 nA) to bring the neuron to threshold. The enhanced conductances that are observed *in vivo* are not mimicked by this depolarization (Pare et al., 1998; Destexhe and Pare, 1999). Superimposed on this steady-state depolarization was a sine wave stimulus (Grass Instruments wave form generator) systematically varied in both frequency (0.2–200 Hz) and amplitude (peak-to-peak, 0.1–0.5 nA). Additionally, the magnitude of the steady-state depolarization was systematically varied to study how the level of activation of an individual neuron affects its frequency following capabilities.

For intracellular recording, sharp microelectrodes were pulled from medium-walled glass (1BF100; WPI) on a Sutter Instruments P-80 micropipette puller and beveled on a Sutter Instruments beveller to a final resistance of 80–120 M $\Omega$ . Electrodes were filled with 2 M potassium acetate with 1.5–2% (wt/vol.) biocytin for subsequent histological identification of recorded cells, all neurons were determined to be pyramidal ( $n=13$  of 13). Recordings were made at 34–36 °C. Data were collected via an Axoclamp 2B intracellular amplifier (Axon Instruments) and digitized at 44 kHz (Neuro-Corder DR-886, Neuro Data Instruments Corp.) and recorded to VCR tapes for subsequent off-line analysis. Analysis was done offline using the Spike2 data collection system (Cambridge Electric Design) or Axoscope 8.0 (Axon Instruments). Statistics were computed using Microsoft Excel or Statview on a PC. Data are reported as means  $\pm$  one standard deviation.

### 4.3. The model

The basic equations for the theta-model itself can be written quite simply as:

$$d\theta/dt = \kappa(1 - \cos\theta) + (1 + \cos\theta)(I_{\text{input}}(t)) \quad (11)$$

$$I_{\text{input}}(t) = \beta + a_{\text{DC}}I_{\text{DC}}(t) + a_{\text{AC}}\sin(\nu t) \quad (12)$$

In Eq. (11),  $\theta$  is the “phase” of the neural membrane potential along its firing cycle (with the spike occurring when  $\theta = \pi$ ),  $\kappa$  determines the spike width at half-amplitude, and  $I_{\text{input}}(t)$  is the injected input. The first term on the right-hand side of Eq. (1) reflects the non-linear dynamics of spike generation, while the second term gives the effect of the inputs on the phase variable  $\theta$ . Both of these terms are given by the reduction method. The parameter  $\kappa$  determines the temporal scale of the spike-generating mechanism, which can be loosely translated into spike width (width measured at half-amplitude). In Eq. (12), the constant bias term  $\beta$  determines

if the model is in an excitable or oscillatory regime:  $\beta < 0$ , the neuron is excitable with a rest state and has threshold for spike initiation;  $\beta > 0$ , the neuron is repetitively firing with frequency proportional to  $\beta^{1/2}$ .  $I_{DC}(t)$  is a constant DC current injection with amplitude  $a_{DC}$ , starting at a pre-set time  $t_1$  and lasting for a defined duration (usually 1 s); the following term is a sinusoid current injection of a frequency  $\nu$  and amplitude  $a_{AC}$ .

To study spike frequency adaptation observed in our neurophysiological recordings, we adapted the basic theta model to include slower currents that modify neural excitability (e.g., AHP currents):

$$d\theta/dt = \kappa(1 - \cos\theta) + (1 + \cos\theta)(I_{input}(t) - g_{slow}Z) \quad (13)$$

$$dz/dt = D(\theta)(1 - z) - z/\tau_z \quad (14)$$

$$D(\theta) = \alpha \exp(-b(1 - \cos(\theta - \theta_T))) \quad (15)$$

Here all the variables are defined as above except for;  $z$  is a slow negative feedback (e.g., AHP current) with strength  $g_{slow}$ . In Eq. (14),  $\tau_z$  is the slow time constant and the function  $D(\theta)$  gives the activation kinetics of  $z$ . In Eq. (15),  $\alpha$  and  $b$  are parameters set to give the appropriate activation kinetics to mimic AHP currents and  $\theta_T$  is the threshold for activation of the slow current. Since cortical pyramidal neurons show varying levels of spike frequency adaptation, we use the modified version of the theta-model in this work. The level of spike frequency adaptation was determined by adjusting the magnitude of the adaptation current,  $g_{slow}$ . This magnitude was adjusted so as to obtain various levels of spike frequency adaptation which results in altered FI curves (see Fig. 1E).

In order to corroborate our study of how the spike generation time scale affects the phase-locking, we used a further variant of the  $\theta$ -neuron that included an additional term that allowed for a precise control of the speed of spike onset. This variant of the theta-neuron was previously used in Naundorf et al. (2005) to study how spike generation speed affects filtering properties of neurons. The model is governed by the following equations:

$$d\theta/dt = \kappa(1 - \cos\theta) + (1 + \cos\theta)(I_{input}(t) - g_{slow}Z) + a_{Na}Na(\theta) \quad (16)$$

$$dz/dt = D(\theta)(1 - z) - z/\tau_z \quad (17)$$

$$D(\theta) = \alpha \exp(-b(1 - \cos(\theta - \theta_T))) \quad (18)$$

$$Na(\theta) = 1 + \tanh[b_{Na}*(\tan(\theta/2))] \quad (19)$$

In Eq. (16), we add a heuristic model of the sodium activation to Eq. (3). Note that Eqs. (16), (17) and (18) are identical to the model above, except for the last term on the right-hand side of Eq. (16). This term gives the speed of the activation of the “sodium current”. Eq. (19) gives the formula of how this current depends on the state variable  $\theta$ ;  $b_{Na}$  is a parameter that controls the gain of this “activation” function. The stronger this current is, the sharper is the onset of the spike (when  $\theta$  goes from rest towards  $\pi$ ). For all simulations using this version of the model, parameters were kept as above, with  $b_{Na}$  set at 20.

In order to measure the speed of the spike onset, we can follow the method suggested by Naundorf et al. (2006). First we

plot a phase-plane for the model, meaning we plot the “current” vs. the “voltage”. For the theta-neuron, we plot the right-hand side of the phase equation ( $\theta_{dot}(t) = \kappa(1 - \cos\theta) + (1 + \cos\theta)(I_{input}(t) - g_{slow}Z(\theta) + \alpha_{Na}Na(\theta))$ ) as a function of  $\theta(t)$ . Then we can calculate, the slope of the trajectory at the spike onset (near  $\theta = 0$ ). This number now quantifies how fast the spike rises off the “floor”. See Fig. 1G for example.

In the present study the models were run with sinusoid inputs with different amplitudes and frequencies. For all the simulations presented  $\tau_z = 200$ ,  $\alpha = 8$ ,  $\beta = 2$ ,  $\theta_T = 3$ ;  $\kappa$ ,  $\alpha$ , and frequency ( $\nu$ ) were varied as marked in figures. To compute the devil’s staircase, the model was integrated using the fourth order Runge–Kutta method using the differential equation analysis software XPPAUT (Ermentrout, 2002).

The infinitesimal phase–response curves (PRCs) we computed using the adjoint method with the XPP software (see Ermentrout, 1996 for mathematics behind the method).

After an initial transient, the model approached either a locked or intermittent spiking response, to compare with the experimental measurements the number of spikes per stimulus cycle were counted and used to compile the devil’s staircase. We also plotted the fraction of spikes per stimulus cycle for every interspike interval (ISI): instantaneous frequency (1/ISI) divided by the input frequency or the ISI/input frequency (see figure captions). This allowed us to observe the intermittency of firing in the unlocked regimes. Averages of such data at a given input frequency recovers the ‘devil’s staircase’ plots.

## Acknowledgments

Thanks to David McCormick for providing the experimental setup. Thanks to Drs. G. Bard Ermentrout, David J. Pinto, Raddy L. Ramos and Peter Latham for helpful comments on the manuscript. BSG was partially funded by the Gatsby Charitable Foundation and the NSF bioinformatics postdoctoral fellowship. JCB was funded by NIMH-K01 MH01944-01A1 and PSC-CUNY 6637-00-35,36.

## Appendix A. The conductance-based neuron

The current conservation equation is:

$$C \frac{dV}{dt} = -(g_{Na}h m^3(V - E_{Na}) + g_K n^4(V - E_K) + g_l(V - E_l) + I_{Ca} + I_{AHP} + I_M) + I_{DC} + I_{per}$$

where the various cross-membrane currents are: DC steady-state current  $I$ , used to set a basal firing rate of the model,  $C$  represents membrane capacitance set at 1 pF/cm<sup>2</sup>.

The periodic input current used to simulate sine wave current injections with amplitude  $A_{per}$ :

$$I_{per} = A_{per} \sin(\text{freq} * 2\pi / 1000)$$

The basic spike-generating currents and leak are the first 3 currents: where  $E_l$  represents resting membrane potential set

at  $-67$  mV,  $E_{Na}=50$  mV,  $E_K=-120$  mV. The maximal conductances are set at  $g_l=0.2$  pS,  $g_k=80$  pS,  $g_{Na}=100$  pS.

The kinetics of the various activation and inactivation variables are:

$$\frac{dm}{dt} = \alpha_m(V)(1 - m) - \beta_m(V)m$$

$$\frac{dn}{dt} = \alpha_n(V)(1 - n) - \beta_n(V)n$$

$$\frac{dh}{dt} = \alpha_h(V)(1 - h) - \beta_h(V)h$$

where:

$$\alpha_m(V) = 0.35(54 + V)(1 - \exp(-(V + 54)/4))$$

$$\beta_m(V) = 0.28(27 + V)(1 - \exp((V + 27)/5) - 1)$$

$$\alpha_n(V) = 0.32(52 + V)(1 - \exp(-(V + 52)/5))$$

$$\beta_n = 0.5\exp(-(57 + V)/40)$$

$$\alpha_h(V) = 0.128\exp(-(50 + V)/18)$$

$$\beta_h(V) = 4.0/(1.0 + \exp(-(V + 27)/5))$$

The  $Ca^{2+}$  current:

$$I_{Ca} = g_{Ca}m_l^\infty(V - E_{Ca})$$

where

$$m_l^\infty = 1 / (1 + \exp(-(V - V_l^{thr})/V_{shp}))$$

The  $Ca^{+}$ -dependent  $K^{+}$ -current which is responsible for the AHP.

$$I_{AHP} = g_{AHP}(Ca/(Ca + K_D))(V - E_K)$$

where:

$$\frac{dCa}{dt} = \alpha I_{Ca} - Ca/\tau_{Ca}$$

The Muscarine-sensitive  $K^{+}$ -current:

$$I_M = g_M w(V - E_K)$$

where:

$$\frac{dw}{dt} = (w_\infty(V) - w)/\tau_w(V)$$

$$\tau_w(V) = \tau_w / (3.3\exp((V - V_w^{thr})/20.0) + \exp(-(V - V_w^{thr})/20.0))$$

$$w_\infty = 1.0 / (1.0 + \exp(-(V - V_w^{thr})/10.0))$$

The parameters for the simulations are as follows:

$E_K = -100$ mV	$E_{Na} = 50$ mV	$E_l = -67$ mV	$E_{Ca} = 120$ mV
$g_l = 0.2$ pS	$g_k = 80$ pS	$g_{Na} = 100$ pS	
$C = 1$ pF/cm <sup>2</sup>	$g_{AHP} = 0$	$g_{Ca} = 1$ pS	
$K_D = 1$	$\alpha = 0.002$	$\tau_{Ca} = 80$	$\phi = 4$
$v_{shp} = 2.5$ mV	$v_{lth} = -25$ mV	$v_{thr} = -10$ mV	
$v_w^{thr} = -35$ mV	$\tau_w = 100$ ms		

$I_{DC}$	set as desired (0 to 10)
freq	set as desired (0 to 100 Hz)
$A_{per}$	set as desired (0 to 10)
$g_m$	set as desired (0 to 1 pS)

REFERENCES

Alexander, J.C., Doedel, E.J., Othmer, H.G., 1990. On the resonance structure in a forced excitable system. *SIAM J. Appl. Math.* 50 (5), 1373–1418.

Amitai, Y., 1994. Membrane potential oscillations underlying firing patterns in neocortical neurons. *Neuroscience* 63 (1), 151–161.

Borg-Graham, L., 1998. Interpretations of data and mechanisms for hippocampal pyramidal cell models chapter in cerebral cortex. In: Ulinski, P.S., Jones, E.G., Peters, A. (Eds.), *Cortical Models*, vol. 13. Plenum Press.

Brown, E., Moehlis, J., Holmes, P., 2004. On the phase reduction and response dynamics of neural oscillator populations. *Neural Comput.* 16 (4), 673–715 (Apr).

Brumberg, J.C., 2002. Firing pattern modulation by oscillatory input in supragranular pyramidal neurons. *Neuroscience* 114, 239–246.

Brumberg, J.C., Nowak, L.G., McCormick, D.A., 2000. Ionic mechanisms underlying repetitive high frequency burst firing in cortical neurons. *J. Neurosci.* 20, 4829–4843.

Carandini, M., Mechler, F., Leonard, C.S., Movshon, J.A., 1996. Spike train encoding by regular-spiking cells of the visual cortex. *J. Neurophysiol.* 76, 3425–3441.

Coombes, S., Bressloff, P.C., 1999. Mode locking and Arnold tongues in integrate-and-fire neural oscillators. *Phys. Rev., E Stat. Phys. Plasmas Fluids Relat. Interdiscip. Topics* 60, 2086–2096.

Desmaisons, D., Vincent, J.D., Lledo, P.M., 1999. Control of action potential timing by intrinsic subthreshold oscillations in olfactory bulb output neurons. *J. Neurosci.* 15 (19(24)), 10727–10737.

Destexhe, A., Pare, D., 1999. Impact of network activity on the integrative properties of neocortical pyramidal neurons in vivo. *J. Neurophysiol.* 81, 1531–1547.

Destexhe, A., Contreras, D., Steriade, M., Sejnowski, T.J., Huguenard, J.R., 1996. In vivo, in vitro, and computational analysis of dendritic calcium currents in thalamic reticular neurons. *J. Neurosci.* 16, 169–185.

Ermentrout, G.B., 1996. Type I membranes, phase resetting curves and synchrony. *Neural Comput.* 8 (5), 979–1003.

Ermentrout, G.B., 2002. *Simulating, Analyzing, and Animating Dynamical Systems: A Guide to XPPAUT for Researchers and Students*. SIAM books.

Ermentrout, G.B., Kopell, N., 1984. Frequency plateaus in a chain of weakly coupled oscillators, I. *SIAM. J. Math. Anal.* 15 (2), 215–237.

Ermentrout, B., Pascal, M., Gutkin, B., 2001. The effects of spike frequency adaptation and negative feedback on the synchronization of neural oscillators. *Neural Comput.* 13 (6), 1285–1310.

Fellous, J.-M., Houweling, A.R., Modi, R.H., Rao, R.P.N., Tiesinga, P.H.E., Sejnowski, T.J., 2001. Frequency dependence of spike timing reliability in cortical pyramidal neurons and interneurons. *J. Neurophysiol.* 85, 1782–1787.

Fourcaud-Trocme, N., Hansel, D., van Vreeswijk, C., Brunel, N., 2003. How spike generation mechanisms determine the neuronal response to fluctuating inputs. *J. Neurosci.* 23 (37), 11628–11640.

Gerstner, W., Kistler, W.M., 2002. *Spiking Neuron Models: Single Neurons, Populations, Plasticity*. Cambridge University Press, Cambridge UK.

Glass, L., Mackey, M.C., 1988. *From Clocks to Chaos*. Princeton University Press, Princeton.

Glass, L., Graves, C., Petrillo, G.A., Mackey, M.C., 1980. Unstable dynamics of a periodically driven oscillator in the presence of noise. *J. Theor. Biol.* 86, 455–475.

Gupta, A., Wang, Y., Markram, H., 2000. Organizing principles for a diversity of GABAergic interneurons and synapses in the neocortex. *Science* 287, 273–278.

- Gutkin, B.S., 1999. A Theory of Action Potential Generation in Cortical Neurons and its Implication for Neural Activity, Doctoral Dissertation, University of Pittsburgh.
- Gutkin, B.S., Ermentrout, G.B., 1998a. Dynamics of membrane excitability determine interspike interval variability: a link between spike generation mechanisms and cortical spike train statistics. *Neural Comput.* 10 (5), 1047–1065.
- Gutkin, B.S., Ermentrout, G.B., 1998b.  $\Theta$ -neuron, a 1-dimensional spiking model that reproduces *in vitro* and *in vivo* spiking characteristics of cortical neurons. In: Paton, H.A. (Ed.), *Information Processing in Cells and Tissues*. Plenum Press, New York, pp. 57–68.
- Gutkin, B.S., Ermentrout, G.B., Reyes, A., 2005. Phase-response curves give the responses of neurons to transient inputs. *J. Neurophysiol.* 94 (2), 1623–1635.
- Guttman, R., Feldman, L., Jakobson, E., 1980. Frequency entrainment of squid axon membrane. *J. Membr. Biol.* 56, 9–18.
- Hansen, A.J., 1985. Effect of anoxia on ion distribution in the brain. *Physiol. Rev.* 65, 101–148.
- Hayashi, H., Ishizuka, S., 1992. Chaotic nature of bursting discharges in the *Onchidium* pacemaker neuron. *J. Theor. Biol.* 156, 269–291.
- Hodgkin, A.L., 1948. The local electric changes associated with repetitive action I a non-medullated axon. *J. Physiol. (London)* 107, 165–181.
- Holden, A.V., 1976. The response of excitable membrane models to a cyclic input. *Biol. Cybern.* 21 (1), 1–7.
- Hoppensteadt, F.C., Izhikevich, E.M., 1997. *Weakly Connected Neural Networks*. Springer-Verlag, New York.
- Hunter, J.D., Milton, J.G., Thomas, P.J., Cowan, J.D., 1998. Resonance effect for neural spike time reliability. *J. Neurophysiol.* 80, 1427–1438.
- Hutcheon, B., Yarom, Y., 2000. Resonance, oscillation and the intrinsic frequency preferences of neurons. *Trends Neurosci.* 23 (5), 216–222 (Related Articles).
- Hutcheon, B., Miura, R.M., Puil, E., 1996. Subthreshold membrane resonance in neocortical neurons. *J. Neurophysiol.* 76, 683–698.
- Izhikevich, E.M., 2000. Neural excitability, spiking and bursting. *Int. J. Bifurc. Chaos Appl. Sci. Eng.* 10, 1171–1266.
- Izhikevich, E.M., 2007. *Dynamical Systems in Neuroscience: The Geometry of Excitability and Bursting*. MIT press.
- Lampl, I., Yarom, Y., 1997. Subthreshold oscillations of the membrane potential and resonant behavior: two manifestations of the same mechanism. *Neuroscience* 78, 325–341.
- Llinas, R.R., Grace, A.A., Yarom, Y., 1991. *In vitro* neuron in mammalian cortical layer 4 exhibit intrinsic oscillatory activity in the 10- to 50-Hz range. *PNAS* 88, 897–901.
- Mainen, Z.F., Joerges, J., Huguenard, J., Sejnowski, T.J., 1995. A model of spike initiation in neocortical pyramidal neurons. *Neuron* 15, 1427–1439.
- McCormick, D.A., Connors, B.W., Lighthall, J.W., Prince, D.A., 1985. Comparative electrophysiology of pyramidal and sparsely spiny stellate neurons of the neocortex. *J. Neurophysiol.* 54, 782–806.
- Naundorf, B., Geisel, T., Wolf, F., 2005. Action potential onset dynamics and the response speed of neuronal populations. *J. Comput. Neurosci.* 18 (3), 297–309.
- Naundorf, B., Wolf, F., Volgushev, M., 2006. Unique features of action potential initiation in cortical neurons. *Nature* 440 (7087), 1060–1063.
- Nowak, L.G., Sanchez-Vives, M.V., McCormick, D.A., 1997. Influence of low and high frequency inputs on spike timing in visual cortical neurons. *Cereb. Cortex* 7, 487–501.
- Nowak, L.G., Azouz, R., Sanchez-Vives, M.V., Gray, C.M., McCormick, D.A., 2003. Electrophysiological classes of cat primary visual cortical neurons *in vivo* as revealed by quantitative analyses. *J. Neurophysiol.* 89, 1541–1566.
- Pare, D., Shink, E., Gaudreau, H., Destexhe, A., Lang, E.J., 1998. Impact of spontaneous synaptic activity on the resting properties of cat neocortical pyramidal neurons *in vivo*. *J. Neurophysiol.* 79, 1450–1460.
- Parmananda, P., Mena, C.H., Baier, G., 2002. Resonant forcing of a silent Hodgkin–Huxley neuron. *Phys. Rev., E Stat. Phys. Plasmas Fluids Relat. Interdiscip. Topics* 66.
- Richardson, M.J., Brunel, N., Hakim, V., 2003. From subthreshold to firing-rate resonance. *J. Neurophysiol.* 89 (5), 2538–2554 (May).
- Rinzel, J., Ermentrout, B., 1998. Analysis of neural excitability and oscillations. In: Koch, C., Segev, I. (Eds.), *Methods in Neuronal Modelling*, The MIT Press, Cambridge, pp. 251–291.
- Rudy, B., McBain, C.J., 2001. Kv3 channels: voltage-gated K<sup>+</sup> channels designed for high-frequency repetitive firing. *Trends Neurosci.* 24, 517–526.
- Schaus, M.J., Moehlis, J., 2006. On the response of neurons to sinusoidal current stimuli: phase response curves and phase-locking. *Proceedings of the IEEE 45th Conf. on Decision and Control*, pp. 2376–2381.
- Smith, G.D., Cox, C.L., Sherman, S.M., Rinzel, J., 2000. Fourier analysis of sinusoidally driven thalamocortical relay neurons and a minimal integrate-and-fire-or-burst model. *J. Neurophysiol.* 83, 588–610.
- Traub, R.D., Jefferys, J.G., Whittington, M.A., 1999. *Fast oscillations in cortical circuits*. MIT Press, Cambridge, MA.
- Volgushev, M., Chistakova, M., Singer, W., 1998. Modification of discharge patterns of neocortical neurons by induced oscillations of the membrane potential. *Neuroscience* 83, 15–25.